Shaft diameter measurement using digital image composition at two different object distances

IOP Conf. Series: Materials Science and Engineering **504** (2019) 012097 doi:10.1088/1757-899X/504/1/012097

Shaft diameter measurement using digital image composition at two different object distances

F Hao[1], J J Shi[1], D L Chen[1], F Wang[1] and Y T Hu[1]

[1]Key Laboratory of Rail Transit Equipment, Nanjing Institute of Technology, Nanjing 211167, China

Corresponding author and e-mail: F Hao, feehao2012@163.com

Abstract. A new machine vision measuring scheme was presented to improve the measurement accuracies of machine vision systems with an ordinary industrial lens and thus to address the extensive requirements for accurately measuring the diameter of shafts. First, method for measuring diameters based on two images was derived on the basis of a pinhole imaging principle, similar triangles and tangent property theorems. Then, a machine vision measuring system was introduced. Finally, experiments were performed on a transmission screw, and the results indicate that the method has achieved a higher measurement accuracy, with systematic errors of approximately 2 μm and uncertainties of 4.9 μm.

1. Introduction

Shafts are important mechanical components, which are commonly used in machinery. The geometric dimensioning and tolerance of shafts have significant effects on the kinematic performance and the service life of a machine. Simultaneously, they also have significant effects on energy savings and environmental protection. Therefore, total and efficient on-line measurement of the accuracy of shafts is important.

The machine vision measuring (MVM) technique is a noncontact measurement method which takes images as transfer carriers of measurements and information. Therefore, it has been used for geometric accuracy in measuring mechanical parts [1]. The commonly used bi-dimensional MVM systems may be subdivided into two categories: the telecentric vision (TLV) system and the pinhole vision (PHV) system. As a benefit of the special optical design of a telecentric lens, magnifications of TLV systems are invariant with a small change in the object distance; therefore, TLV systems can achieve high accuracy and usually micron class accuracy [2, 3]. However, the field-of-view (FOV) of TLV systems is relatively small since only light rays that are parallel to the principal optic axis can be passed through the lens to illuminate the image plane. Therefore, a PHV system has a wider FOV than a TLV system when the lens dimensions of the PHV system and the TLV system are approximately equal. According to the pinhole camera model, light rays are tangent to the cylindrical surface of the shaft. The image of the shaft corresponds to the minor arc $\widehat{ab}$, and the pixel equivalent coefficient method cannot be used to obtain correct measurements. The incorrect results were defined by Tan et al. as pseudo-diameter. Wei and Tan proposed that the intrinsic and extrinsic parameters can be sequentially calibrated using Zhang's method [4] and using a shaft of known diameter. The Levenberg-Marquardt algorithm was selected to solve the extrinsic parameters. The measurement accuracy was improved by

controlling the illumination area and weakening the fringe effect. Experimental results show that if the diameters of the shafts are between ϕ30 mm and ϕ40 mm, measuring errors are less than 0.015 mm [5]. However, the distance between the camera and the shaft must be equal to the distance between the camera and the calibration shaft during the entire measurement process, but it is difficult to guarantee that the two distances are equal. Sun et al. established a vision measurement model for shaft parts on the basis of the pinhole imaging principle and geometrical constraints such as tangency and/or perpendicularity. The measurement system was calibrated using a plane calibration target fixed in a specific location. The mean measurement error of the system was approximatively 0.005 mm [6]. A datum plane was adopted, and thus, an error correction model was established on the basis of the distance between the datum plane and the camera. Experimental results on measured shafts with nominal diameters from ϕ2 mm to ϕ10 mm show that the measurement errors are within 0.009 mm [7]. Based on the above results, we can conclude that the higher measurement accuracy was achieved by the TLV measurement method. However, a TLV system should be configured with an appropriately sized telecentric lens according to the dimensions of the measured shaft. The PHV system has a wider FOV than the TLV system, and its measurement accuracy would be significantly improved by introducing geometrical constraints to the imaging model. However, Sun's method [6] requires that the calibration target should be fixed in a particular location. Motivated by Sun's method, a new PHV-based measuring scheme will be proposed in this paper. Similarly, the geometrical constraints will also be employed to improve the performance of the method. One of the most prominent characteristics is that two digital images under different object distances will be utilized so that four points are adopted to measure the shaft diameter.

The remainder of the paper is structured as follows: Section 2 introduces the mathematical model for measuring shaft diameters and as well as the developed MVM system. Experimental results and a comparison study with CMMs are presented in Section 3. Concluding remarks are given in Section 4.

2. Measuring principle and measuring system

As shown in Figure 1, the coordinates of tangent point a_1 and the camera's optical center point are (x_a, y_a, z_a) and (x_c, y_c, z_c), respectively, in the world coordinate system (WCS) o_w-$x_w y_w z_w$. $o(x, y, z)$ is the center of the section circle. a_2 is another tangent intersection point of the light ray and measured shaft.

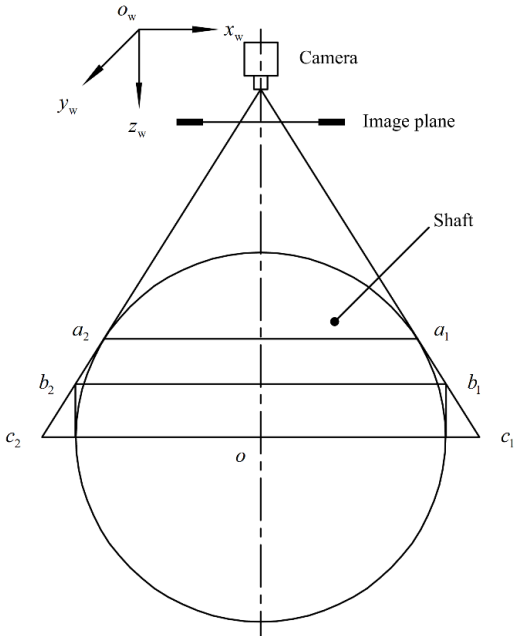

Figure 1. Radial direction imaging model of a shaft.

Given that translation transformation is only involved between the camera coordinate system (CCS) and WCS, the relationship between the world coordinates and the pixel coordinate of a_1 can be formulated as:

$$\begin{cases} u_a = (x_a - x_c / z_a - z_c) \cdot (f/dx) + u_0 \\ v_a = (y_a - y_c / z_a - z_c) \cdot (f/dy) + v_0 \end{cases} \tag{1}$$

where dx and dy are the center-to-center distances between pixels in the row and column directions, respectively; f is the focal length; (u_0, v_0) is the origin of the image coordinate system in the pixel coordinate system; and (u_a, v_a) is the pixel coordinate of a_1.

According to the tangency condition of the light rays and the shaft, one equation can be obtained as follows:

$$(x_a - x_c)(x_a - x) + (z_a - z_c)(z_a - z) = 0 \tag{2}$$

With the geometrical constraint that the tangent point a_1 belongs to the section circle, *Eq*. (3) can be obtained.

$$(x_a - x)^2 + (y_a - y)^2 + (z_a - z)^2 = r^2 \tag{3}$$

where r is the radius of the section circle.

β_a is the measurement scale along the x_w-axis of the system at location a_1a_2, and β_c is the measurement scale along the x_w-axis at location c_1c_2. Please refer to our previous work [8] for a detailed process for deriving the measurement scale. Given that the length of the minor arc c_1c_2 in the pixel coordinate system is P pixels, two diameters can be estimated by

$$\tilde{d}_1 = P \cdot \beta_a = [z_a - z_c / f] \cdot P \cdot d_x \tag{4}$$

$$\tilde{d}_2 = P \cdot \beta_c = [z - z_c / f] \cdot P \cdot d_x \tag{5}$$

where $\tilde{d}_1$ and $\tilde{d}_2$ are estimation values of the measured shaft diameter d.

Actually, $\tilde{d}_1$ is the length of the line segment a_1a_2, and $\tilde{d}_2$ is the length of the line segment c_1c_2. Therefore, the inequality $\tilde{d}_1 < d < \tilde{d}_2$ is satisfied. Assuming there exists a location b_1b_2 between a_1a_2 and c_1c_2 and the measurement scale along the x_w-axis of the system at b_1b_2 between them is β_b, as shown in Figure 1, a new estimation value of d can be obtained that is exactly equal to the true value. β_b can be denoted by the weighted average of β_a and β_c.

$$\beta_b = \beta_c (1 - \lambda) + \beta_a \lambda \tag{6}$$

where λ is the weight, and its bounds are greater than 0 and less than 1.

Based on the pinhole camera model, λ can also be calculated by

$$\lambda = \frac{4 - \sqrt{16 - 4\gamma^2}}{\gamma^2} \tag{7}$$

where γ is equal to the ratio of the diameter d to the object distance D. As γ decreases with increasing D, the weight λ decreasingly approaches 0.5.

Here, the diameter can be re-estimated by

$$\tilde{d}_3 = P\beta_b = P[\beta_c (1 - \lambda) + \beta_a \lambda] \tag{8}$$

where $\tilde{d}_3$ is the estimation value of the measured shaft diameter d.

According to the imaging model shown in Figure 1, these implied conditions hold, i.e., $x = x_c$, $y = y_c$, and $y_a = y_c$.

By solving the simultaneous equations of *Eq*. (1) to *Eq*. (3), *Eq*. (8) and the implied conditions, λ can also be expressed as

$$\lambda = \frac{\omega^2 - 2\sqrt{\omega^2 + 4} + 4}{\omega^2} \tag{9}$$

where ω is equal to the ratio of the pixel length P to the x-direction effective focal length f_x, which is equal to the ratio of f to d_x.

Two images are acquired with different object distances, D_1 and D_2, and are processed sequentially by image preprocessing, feature detection, and feature computation; therefore, two pixel lengths, P_1 and P_2, are obtained. Substituting P_1 and P_2 into *Eq*. (9) yields λ_1 and λ_2 and then γ_1 and γ_2 on the basis of *Eq*. (7). Then, the diameter d can be estimated by *Eq*. (10).

$$\tilde{d} = C \cdot \frac{\gamma_2 \gamma_1}{\gamma_2 - \gamma_1} \tag{10}$$

where C is a constant which is equal to the difference between D_1 and D_2. $\tilde{d}$ is the new estimation value of the measured shaft diameter d.

As illustrated in Figure 2, an MVM system was developed to verify the measurement principle stated above. The main parameters of our camera are as follows: the size of the image device is 2/3 inches; the image sizes are 2452 pixels by 2056 pixels in the horizontal and vertical directions, respectively; and the pixel sizes are 3.45 μm × 3.45 μm. Two square LED arrays were symmetrically installed to illuminate the measuring field to acquire sufficiently detailed information. The positioning of the LED lights was studied to achieve uniform illumination, which can be used to acquire high-quality images.

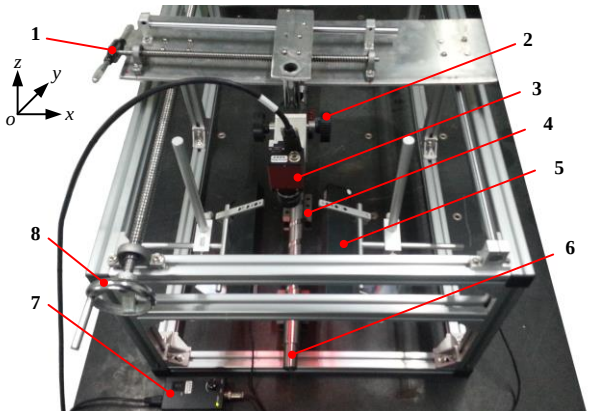

Figure 2. MVM system for shafts
1 *x*-direction regulating handle; 2 *z*-direction regulating handle; 3 AVT Stingray F-504B Camera; 4 encoded V-block; 5 Square LED array; 6 Measured shaft; 7 LED light controller; 8 *y*-direction regulating handle

3. Experimental results

Extensive experiments were carried out to verify the performance of the proposed MVM method in comparison to CMM. The transmission screw was employed in the experiments. The screw includes four segments, i.e., two shaft journals, a shaft head, and the threaded segment. The nominal diameter of the threaded segment is ϕ30 mm, and the length is 876 mm. Nine measuring points were distributed on the threaded segment. Nine measurements were conducted at each point. Measurement results are shown in Table 1. μ is the mean of the nine measurements, and σ is the standard deviation. u_A is the type A uncertainty, and U_{95} is the expanded uncertainty when the confidence level is 95%. It should be noted that only u_A was considered when calculating the combined standard uncertainty u_c [9].

Table 1. Comparison of CMM and MVM measuring results.

Points	Measuring Results of CMM [mm]				Measuring Results of MVM [mm]				Systematic Error [μm]
	Mean μ	Std. σ	u_A	U_{95}	Mean μ	Std. σ	u_A	U_{95}	
1	29.9383	0.00335	0.00112	±0.00223	29.9375	0.00794	0.00265	±0.00529	0.8
2	29.9407	0.00264	0.00088	±0.00176	29.9393	0.00643	0.00214	±0.00429	1.4
3	29.9508	0.00335	0.00112	±0.00223	29.9504	0.00518	0.00173	±0.00345	0.4
4	29.9544	0.00263	0.00093	±0.00186	29.9533	0.00657	0.00232	±0.00465	1.1
5	29.9589	0.00354	0.00125	±0.00250	29.9603	0.00972	0.00344	±0.00688	1.4
6	29.9575	0.00368	0.00123	±0.00245	29.9552	0.00685	0.00228	±0.00457	2.3
7	29.9670	0.00384	0.00128	±0.00256	29.9725	0.00594	0.00198	±0.00396	5.5
8	29.9665	0.00372	0.00124	±0.00248	29.9673	0.00818	0.00273	±0.00545	0.8
9	29.9649	0.00445	0.00148	±0.00297	29.9643	0.00838	0.00279	±0.00559	0.6

From the above table, we observe that (1) the U_{95} values of CMM and MVM are ± 2.34 μm and ± 4.9 μm, respectively —, i.e., the half-interval length of MVM is double that of CMM. (2) The maximum systematic error, 5.5 μm, occurs at the 7th measuring point. Excluding the 7th measuring point, the mean of the systematic errors is 1.1 μm. The results indicate that higher measurement accuracy has been achieved by the proposed method.

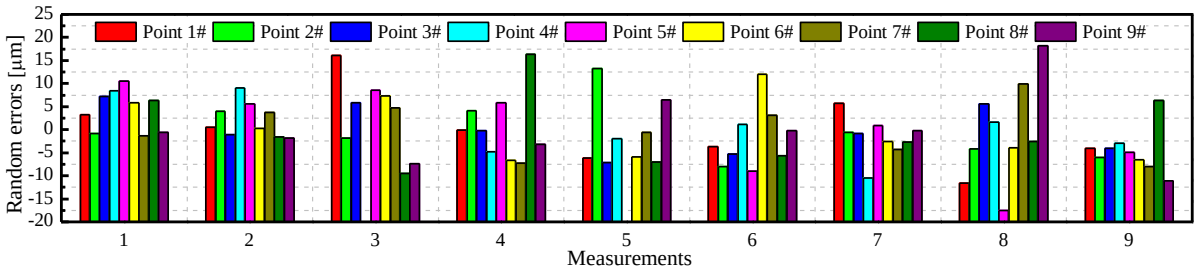

Figure 3. Random errors of MVM at nine measurement points: the colors red, green, blue, cyan, magenta, yellow, dark yellow, olive, and purple correspond to the 1st, 2nd, 3rd, 4th, 5th, 6th, 7th, 8th, and 9th measurement point, respectively.

As illustrated in Figure 3, in all nine measurements at the 1st measuring point, the maximum random error is + 16.1 μm, which occurs during the 3rd measurement, and the second maximum random error is - 11.6 μm, which occurs during the 8th measurement. Excluding the 3rd and 8th measurement results, the range of the remaining random errors is 11.97 μm. For the 2nd measurement point, the maximum random error is + 13.3 μm, which occurs in the 5th repeated measurement. Excluding the 5th measurement result, the range of the remaining random errors is 12.06 μm. For the 3rd measurement point, the range of the nine random errors is 14.31 μm. For the 4th measurement point, the maximum absolute random error occurs in the 7th measurement. Excluding the 7th measurement results, the range of the remaining random errors is 13.88 μm. For the 5th measurement point, the absolute random errors of the 1st and 7th measurements are relatively large, and the maximum error, 17.50 μm, occurs in the 7th measurement. Removing the 1st and 7th measurement results, the range of the remaining random errors is 17.50 μm. For the 6th measurement point, the random error of the 6th measurement is approximately 12 μm, and the range of the remaining eight random errors is 14.02 μm. Compared with the measurement results at the 3rd measurement point, the maximum random error and the range at the 7th measurement point is 2 μm and 3.68 μm larger, respectively. The random error of the 4th repeated measurement at the 8th measurement point is the largest, and its absolute value is 16.3 μm. The range of the eight remaining random errors is 15.9 μm. The random error of the 8th repeated measurement at the 9th measurement point is the highest, and its absolute value is 18.2 μm. The range of the eight remaining random errors is 17.47 μm. Based on the above results, the presented

method has increased the measurement accuracy. With the exception of a few outliers, the ranges of the random errors are within 18 μm. Compared with the measurement results of CMM, the systematic errors are within approximately 2 μm if a few outliers are eliminated.

4. Conclusions

We presented a new MVM scheme using two images at different object distances to measure the diameters of shafts. First, the measurement model was derived on the basis of the pinhole imaging principle combined with some geometrical constraints, including tangency and perpendicularity. An MVM system was developed subsequently. Experiments on a transmission screw and contrast experiments were performed, and the experimental results show the following: (1) the U_{95} values of CMM and MVM are ± 2.34 μm and ± 4.9 μm, respectively —, i.e., the half-interval length of MVM is approximately double that of CMM. (2) In contrast with the measurement results of CMM, the maximum systematic error is 5.5 μm, and the systematic errors are within approximately 2 μm with the elimination of some outliers. (3) With the elimination of some outliers, the range of the random errors is within approximately 18 μm. Consequently, the presented MVM method achieved higher measurement accuracy, and the random errors could be reduced by multiple measurements in laboratories. However, further work is necessary to reduce the random error in a single measurement in uncontrolled circumstances.

Acknowledgement

This work was supported in part by the National Natural Science Foundation of China under Grant No.51705238, the Natural Science Foundation of Higher Education of Jiangsu Province under Grant No.16KJB460012 and 15KJA46007, the Natural Science Foundation of Nanjing Institute of Technology under Grant No. ZKJ201601 and JCYJ201602, and the Key Constructive Discipline of Jiangsu Province under Grant No. JXKJ201509.

References

[1] Mekid S, Ryu H S 2007 Rapid vision-based dimensional precision inspection of mesoscale artefacts. *Proceedings of the Institution of Mechanical Engineers, Part B: Journal of Engineering Manufacture* **221**(4) 659-672

[2] Guo S, Zhang J, Jiang X, Peng Y, Wang L 2011 Mini Milling Cutter Measurement Based on Machine Vision *Procedia Engineering* **15** 1807-1811

[3] Garbacz P, Giesko T 2016 Multi-camera vision system for the inspection of metal shafts *Proc. Int. Conf. on Challenges in Automation, Robotics and Measurement Techniques (Warsaw)* vol 440 (Springer, Cham) 743-752

[4] Zhang Z Y 1999 Flexible camera calibration by viewing a plane from unknown orientations *Proc. Int. Conf. on Computer Vision (Kerkyra)* vol 1 (IEEE Inc) 666-673

[5] Wei G, Tan Q 2011 Measurement of shaft diameters by machine vision *Applied Optics* **50**(**19**) 3246-3253

[6] Sun Q, Hou Y, Tan Q, Li C 2014 Shaft diameter measurement using a digital image *Optics and Lasers in Engineering* **55** 183-188

[7] Wang J, Gao B, Zhang X, Duan X, Li X 2016 Error correction for high-precision measurement of cylindrical objects diameter based on machine vision *Proc. Int. Conf. on Electronic Measurement and Instruments (Qingdao)* vol 3 (IEEE Inc) 1113-1117

[8] Hao F, Zhu, S Q, Gao H T 2014 Gray image composition method for measurement based on multi-software cooperation *Proc. Int. Conf. on Advances in Materials and Manufacturing (Kunming)* vol 889-890 () 1052-1056

[9] Rajan A, Kuang Y C, Ooi M P L Demidenko S N 2016 Benchmark Test Distributions for Expanded Uncertainty Evaluation Algorithms *IEEE Transactions on Instrumentation and Measurement* **65**(**5**) 1022-1034